



HAL
open science

Time-Domain Homogenization of Foil Windings in 2-D Axisymmetric Finite-Element Models

Carlos Valdivieso, Gérard Meunier, Brahim Ramdane, Johan Gyselinck, Christophe Guerin, Ruth Sabariego

► **To cite this version:**

Carlos Valdivieso, Gérard Meunier, Brahim Ramdane, Johan Gyselinck, Christophe Guerin, et al.. Time-Domain Homogenization of Foil Windings in 2-D Axisymmetric Finite-Element Models. IEEE Transactions on Power Delivery, 2021, IEEE Transactions on Power Delivery, 36 (3), pp.1-1. 10.1109/TPWRD.2020.3005225 . hal-03054615

HAL Id: hal-03054615

<https://hal.science/hal-03054615v1>

Submitted on 14 Dec 2020

HAL is a multi-disciplinary open access archive for the deposit and dissemination of scientific research documents, whether they are published or not. The documents may come from teaching and research institutions in France or abroad, or from public or private research centers.

L'archive ouverte pluridisciplinaire **HAL**, est destinée au dépôt et à la diffusion de documents scientifiques de niveau recherche, publiés ou non, émanant des établissements d'enseignement et de recherche français ou étrangers, des laboratoires publics ou privés.

Time-Domain Homogenization of Foil Windings in 2-D Axisymmetric Finite-Element Models

Carlos A. Valdivieso, Gerard Meunier, Brahim Ramdane, Johan Gyselinck, Christophe Guerin,
and Ruth V. Sabariego

Abstract—In this paper, an approach for the time-domain homogenization of foil windings in axisymmetric finite-element (FE) models is presented. The homogenized formulation is characterized by an axial current redistribution due to the skin effect and a radial inter-turn voltage given by the insulation in-between the turns. The method is successfully applied to an axisymmetric 20-turn foil-winding inductor. At low frequencies, the local and global results present an excellent agreement with those obtained by an accurate but expensive FE model in which all turns are explicitly discretized. The air-gap effect and the frequency limitations are studied as well.

Index Terms—Eddy currents, finite element method, foil windings, homogenization, skin effect, time domain.

I. INTRODUCTION

FOIL windings are extensively used in transformers and inductors in a wide range of frequencies and rated powers. For these devices, eddy-current effects are an essential aspect at the design stage. To this end, some analytical, semi-analytical or empirical approaches have been proposed as in [1]–[5]. Numerical methods can also be used, e.g., the Partial Element Equivalent Circuit (PEEC) method [6] or the FE method. Classically, the eddy-current analysis of windings in FE models requires the representation of each separate turn of the winding [7]. For most real-life applications, with possibly complex geometries, this leads to computationally expensive simulations with a prohibitive number of unknowns, specially in full 3-D problems. To overcome this problem, several solutions are proposed in the literature e.g., a semi-numerical approach [8], an acceleration procedure [9] or homogenization techniques [10], [11].

Homogenization techniques dedicated to foil windings so far available in the literature are limited, to the best of our knowledge, to the frequency domain [10], [11]. Time domain

analysis has an important role as well, it allows the representation of transient phenomena (such as e.g., inrush currents), the operation under non-sinusoidal excitations, saturation or non-linearity (windings are mostly linear, but embedded in nonlinear domains). Furthermore, these homogenization techniques have only been validated at utility frequency (50 Hz) [10], [11]. The fringing flux, which has an important influence on gapped foil-winding devices [12], [13], has not been considered either in the homogenized models.

We propose a time-domain extension, through an implicit-euler discretization, of the developments done in [10], [11]. The homogenization is characterized by the assumption of an axial redistribution of the current density in the foil and a radial inter-turn voltage, which are modeled by a simplification of the circuit-coupling equation and a 1-D radial discretization, respectively. Preliminary time-domain results were presented in [14]. In this paper, we apply the axisymmetric homogenized formulation to a gapped 20-turn copper foil-winding inductor, perform an impedance analysis in the frequency domain, study the effect of the fringing flux on the homogenization hypotheses and define the model limitations in frequency. The results are compared to those obtained with a reference brute-force FE model in which all turns are explicitly discretized.

II. MAGNETODYNAMIC FORMULATION

A bounded domain Ω of the Euclidean space is considered. The conducting and nonconducting subdomains are denoted Ω_c and Ω_{nc} respectively, with $\Omega = \Omega_c \cup \Omega_{nc}$. In the \underline{a} - v formulation (vectors denoted by underlined symbols), the electric field \underline{e} is expressed in terms of the magnetic vector potential \underline{a} and the gradient of an electric scalar potential v in Ω_c , i.e.,

$$\underline{e} = -\partial_t \underline{a} - \text{grad } v \text{ in } \Omega_c \quad \text{with} \quad \underline{b} = \text{curl } \underline{a} \text{ in } \Omega, \quad (1-2)$$

so that the Faraday law is satisfied. The current density \underline{j} and the magnetic field \underline{h} are obtained from the constitutive relations, for linear and isotropic materials, $\underline{h} = \nu \underline{b}$ and $\underline{j} = \sigma \underline{e}$, where ν is the magnetic reluctivity and σ the electrical conductivity.

In cylindrical coordinates (r, ϕ, z) , \underline{a} , \underline{e} and \underline{j} get reduced to their ϕ component: a_ϕ , e_ϕ and j_ϕ . A voltage V defines $\text{grad } v = -V/2\pi r$ and $a = ra_\phi$. The magnetic field \underline{h} and the magnetic flux density \underline{b} have components only in the r - z plane. Thus, the Ampere law reads

$$-\partial_r \left(\frac{\nu}{r} \partial_r a \right) - \partial_z \left(\frac{\nu}{r} \partial_z a \right) + \frac{\sigma}{r} \partial_t a - \sigma \frac{V}{2\pi r} = 0. \quad (3)$$

Manuscript received XXXX XX, 2020; revised XXXX XX, 2020. (*Corresponding author: Carlos A. Valdivieso*)

C. A. Valdivieso is with Altair Engineering France, 38240 Meylan, France, and is working towards a joint PhD with KU Leuven, Department of Electrical Engineering, KU Leuven, 3600 Genk, Belgium, and Université Grenoble Alpes, CNRS, Grenoble INP, G2Elab, F-38000 Grenoble, France (e-mail: cvaldivieso@altair.com).

G. Meunier and B. Ramdane are with the Université Grenoble Alpes, CNRS, Grenoble INP, G2Elab, F-38000 Grenoble, France (e-mail: gerard.meunier@grenoble-inp.fr; brahim.ramdane@grenoble-inp.fr).

J. Gyselinck is with the Department of Bio- Electro- And Mechanical Systems, Université libre de Bruxelles, 1050 Brussels, Belgium (e-mail: johan.gyselinck@ulb.ac.be).

C. Guerin is with Altair Engineering France, 38240 Meylan, France (e-mail: cguerin@altair.com).

R. V. Sabariego is with the Department of Electrical Engineering, KU Leuven, 3600 Genk, Belgium (e-mail: ruth.sabariego@kuleuven.be).

For circuit-coupled problems, the total current I_s flowing through a solid conductor is expressed by the relation [15]:

$$\int_{\Omega_c} \left(-\frac{\sigma}{r} \partial_t a + \sigma \frac{V}{2\pi r} \right) d\Omega_c = I_s. \quad (4)$$

III. FOIL WINDING MODEL

A typical foil winding of cylindrical disposition with N_f turns, height l_z , total radial width l_r and fill factor λ is considered. The thickness of the conductive foil l_f can be expressed as $l_f = \lambda l_r / N_f$. Thus, the cross-sectional area of the conductive foil is given by $l_f l_z$. The foil is assumed nonmagnetic (with $\nu = \nu_0 = 1/\mu_0$ and $\mu_0 = 4\pi \cdot 10^{-7}$ H/m) with conductivity σ . The skin depth at frequency f , or pulsation $\omega = 2\pi f$, is given by $\delta = \sqrt{\nu/\pi f \sigma}$ and the reduced frequency is defined as $\zeta = l_f/\delta$. The insulation between the foil turns is also nonmagnetic. Two phenomena are considered in the model: the inter-turn voltage and the skin effect.

A. Inter-turn voltage

In a foil winding, a voltage appears in the radial direction due to the insulation in-between the turns. The voltage V_n for every turn n is assumed constant in the axial direction and within the cross-section of the turn. Hence, the terminal voltage V across the foil winding can be expressed as

$$V = \sum_{n=1}^{N_f} V_n. \quad (5)$$

In the homogenized model, the turns are not geometrically defined. The behavior in (5) is then modeled by an extra 1-D spatial voltage function V_r depending on the radial position r , i.e. $V_n = V_r(r)$, with continuous polynomial variations as possible approximation [11]. This way, V_r extends the inter-turn voltage to a continuum across the winding, so that it is valid for all the N_f turns. The terminal voltage V is approximated with the average value of V_r through the total radial width l_r , which is multiplied by the total number of turns N_f , so that (5) becomes

$$V = \frac{N_f}{l_r} \int_{l_r} V_r dr. \quad (6)$$

B. Skin effect

The skin effect in a conductive foil is predominant along its height, since the thickness of the foil is usually smaller than the skin depth $l_f < \delta$. The current density is concentrated on both axial ends and can be considered constant in the radial direction. The assumption made is that j_ϕ does not vary along the thickness of the foil [10]. The current flowing in every foil turn n is the same and is denoted I_f . Thus, the current for a single turn n can be obtained by simplifying the integral in (4) along the radial direction:

$$\int_{l_z} \left(-\lambda \frac{\sigma}{r} \partial_t a + \lambda \sigma \frac{V_r}{2\pi r} \right) dz = \frac{N_f}{l_r} I_f. \quad (7)$$

C. Discretization

For the magnetic vector potential, a nodal FE function space $F_a(\Omega)$ is defined on a mesh of Ω containing the shape functions α_i and the test functions α_j . The voltage drop V_r is associated to a radial one-dimensional function space $F_V(\Omega_f)$ defined in Ω_f , with $\Omega_f \subset \Omega_c$, where Lagrange polynomials define the shape functions β_k and test functions β_l . The interpolation form is given by

$$V_r = \sum_{k=1}^{N_V} V_{r_k} \beta_k \quad (8)$$

with

$$\beta_k(r) = \prod_{\substack{m=1 \\ m \neq k}}^{N_V} \frac{r - r_m}{r_k - r_m}, \quad (9)$$

where N_V is the number of interpolating points equidistantly spaced through the total width l_r of the winding. Note that the discretization of V_r is independent of the mesh used for the potential quantities.

D. Weak formulation

Applying the Galerkin method to (3), the weak form of the Ampere law is obtained as

$$\int_{\Omega} \frac{2\pi}{r} \nu \text{grad } a \cdot \text{grad } \alpha_j d\Omega + \lambda \partial_t \int_{\Omega_f} \frac{2\pi}{r} \sigma a \alpha_j d\Omega_f - \lambda \int_{\Omega_f} \frac{\sigma}{r} V_r \alpha_j d\Omega_f = 0, \quad \forall \alpha_j \in F_a(\Omega). \quad (10)$$

Likewise, the circuit relation from (7) is multiplied by the test function β_l and integrated over the radial direction, i.e.

$$-\lambda \partial_t \int_{\Omega_f} \frac{\sigma}{r} a \beta_l d\Omega_f + \lambda \int_{\Omega_f} \frac{\sigma}{2\pi r} V_r \beta_l d\Omega_f - \frac{N_f I_f}{l_r} \int_{l_r} \beta_l dr = 0, \quad \forall \beta_l \in F_V(\Omega_f). \quad (11)$$

For a voltage-driven foil winding, (10) and (11) are solved together with the source term (6). Time derivatives are approximated with the implicit-Euler method.

E. Loss & Magnetic Energy

In a homogenized foil-winding domain, the instantaneous Joule losses p and magnetic energy w can be estimated as [17]:

$$p = 2\pi \int_{\Omega_f} r e_\phi j_\phi d\Omega_f. \quad (12)$$

$$w = \pi \partial_t \int_{\Omega_f} r \underline{h} \underline{b} d\Omega_f. \quad (13)$$

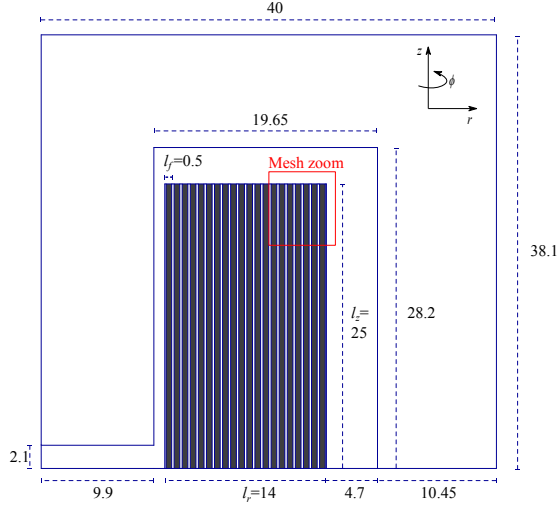


Fig. 1. Axisymmetric foil inductor (upper half, dimensions: mm).

F. Limitations

For a given frequency f , the model assumes that the foil thickness l_f is always smaller than the skin depth δ . It means that the skin effect along the foil thickness is disregarded. In theory, this condition allows the definition of a maximum frequency of application, it reads:

$$f_{max} = \frac{\nu}{\pi\sigma} \left(\frac{N_f}{\lambda l_r} \right)^2, \quad (14)$$

or in terms of the reduced frequency $\zeta_{max} = 1$. Therefore, transient phenomena can be analyzed with the proposed model provided that $f < f_{max}$.

IV. APPLICATION

The proposed method is applied to an axisymmetric FE model of the 20-turn foil inductor shown in Fig. 1. Due to symmetry, only the upper half of the cross-section is considered. A copper foil of thickness $l_f = 0.5$ mm is considered with 0.1 mm insulation layers on each side ($\lambda = 0.71$). The core is considered nonconductive with relative reluctivity $\nu_r = 1/1000$. Third-order polynomials are used for the inter-turn voltage approximation with equidistant interpolating points $r = (10.85, 14.35, 21.35, 24.85)$ mm. The results are compared to those obtained by a FE model with all foils explicitly defined and represented as solid conductors. The reference computations are carried out with the software Altair FluxTM [16], whereas the proposed homogenized approach is developed in the MATLAB environment.

The meshes are defined upon a parameter N_u that defines the number of unknowns within the thickness of each foil turn l_f to properly account for the eddy-current effects. For the reference case, a fixed mesh with $N_u = 5$ is considered to ensure an excellent accuracy up to $\zeta = 2$. As a rule of thumb, 3 unknowns within δ ensure a good estimation of the eddy-current effects [18]. This fine mesh is shown in Fig. 2a and leads to a total of 118298 unknowns, comprising the whole domain of Fig. 1. As for the homogenized case, there is no predefined criteria to assign the number of unknowns over

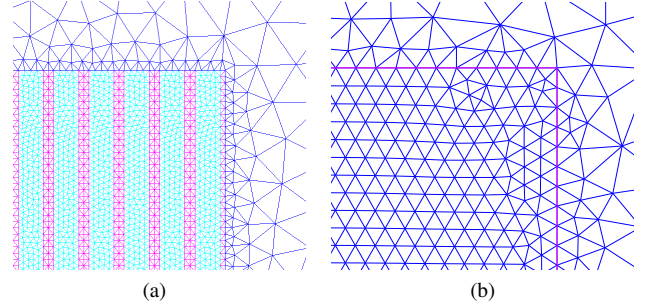


Fig. 2. Detail of the model mesh (upper-right zoom of the outer foil turns): (a) reference case and (b) homogenized case.

the winding region. Thus, it is the intention of this study to evaluate the performance of the homogenization with respect to the number of unknowns N_u . Initially, we arbitrarily set it to $N_u = 2$, but different values (from 1 to 3) are considered further in the analysis. The $N_u N_f$ unknowns are uniformly spanned across l_r as shown in Fig. 2b. This homogenized mesh leads to a total of 4082 unknowns, comprising the whole domain of Fig. 1.

Frequency-domain calculations are first carried out to obtain the terminal resistance R and inductance L as functions of the reduced frequency ζ for both the reference and the homogenized cases. These parameters are obtained from the complex power as

$$R = \text{Re} \left(\frac{|\mathbf{V}|^2}{2(P + \imath Q)} \right), \quad (15)$$

$$L = \text{Im} \left(\frac{|\mathbf{V}|^2}{2(P + \imath Q)} \right) \frac{\sigma l_f^2}{\nu_0 \zeta^2}, \quad (16)$$

where \mathbf{V} is the complex terminal voltage, P the active power, Q the reactive power and \imath the imaginary unit. To investigate the effect of the fringing flux on the impedance, an extra air-gap size of 4.2 mm is considered in this part. For the resistance, good agreement is observed in Fig. 3 until $\zeta = 0.75$ ($f \simeq 13$ kHz). As for the inductance, excellent accuracy is shown for all the considered frequencies. It is worth mentioning that in Fig. 2 the model is only pushed beyond f_{max} to illustrate the limitations in accuracy. In all figures, ‘‘r.’’ stands for the reference model and ‘‘h.’’ for the homogenized model.

In the time domain, three square-wave voltage excitations are applied to the winding, for which the waveform is depicted in Fig. 4. The only difference between the three waves is their fundamental frequency: 200 Hz ($\zeta = 0.107$), 2 kHz ($\zeta = 0.339$) and 20 kHz ($\zeta = 1.071$), where the latter is above the maximum frequency ($f_{max} \simeq 17$ kHz). Time-stepping simulations are carried out for one period ($T = 1/f$) with time step $\Delta t = T/200$. For the reference case, a computational time per step $t_{\Delta t}$ of 5389 ms is obtained at all frequencies. The homogenization requires a $t_{\Delta t}$ of 31 ms at 200 Hz or 2 kHz and 70 ms at 20 kHz. It is important to notice that the homogenized model adds extra unknowns due to the discretization of the inter-turn voltage. The number of extra unknowns depends on the degree of the polynomial used to approximate V_r , which in this case adds 3 extra unknowns.

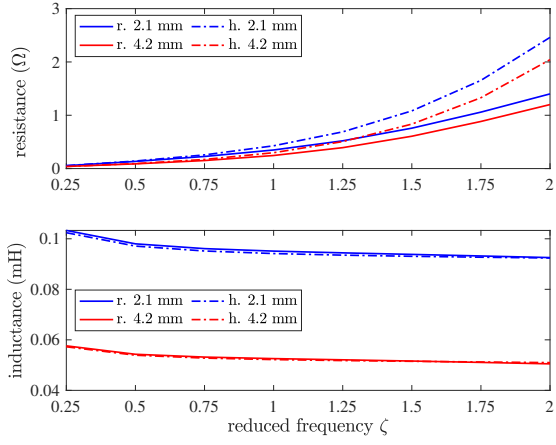


Fig. 3. Terminal resistance and inductance vs reduced frequency ζ .

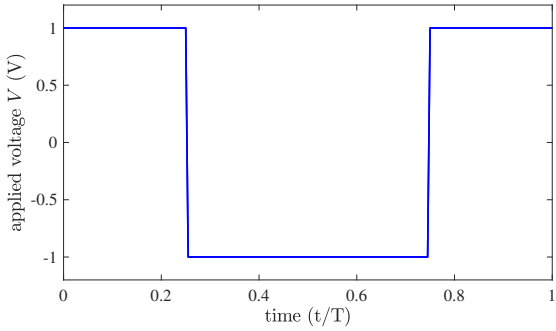


Fig. 4. Applied voltage vs normalized time.

The lowest degree of approximation that can be considered is a first-order polynomial; if a constant approximation is chosen, the model behaves as a solid conductor. For a first-order approximation, $t_{\Delta t}$ is slightly lower: 30 ms at 200 Hz or 2 kHz and 69 ms at 20 kHz; but the results are less precise [11].

The flux lines in the foil-winding domain for the reference and homogenized cases are compared in Fig. 5 at $t = T/8$ (maximum voltage instant) for all frequencies. The inter-turn voltage across the turns of the foil winding is shown in Fig. 6 at instants $t = T/8$ and $t = T/2$ for all frequencies. These time instants are selected to coincide with a peak positive and negative value of the applied voltage. The continuum voltage approximation follows precisely the behavior of the reference case at both times. The terminal voltage can be obtained from the values in Fig. 6 together with (6). It is clear that a first-order approximation would only decrease the model accuracy in exchange of a small reduction in $t_{\Delta t}$.

The current density distribution over the axial direction for the first turn is presented in Fig. 7 at $t = T/8$ and $t = T/2$. The homogenized model depicts correctly the concentration in the middle of the foil as a consequence of the fringing flux coming from the air-gap. Likewise, the current density across the total radial width, for $z = 0$, is also compared in Fig. 8. Here, it can be observed that the current density is not constant within l_f , even at 200 Hz, in the foils closer to the air-gap. In general, the homogenization follows the tendency of the reference. In terms of the current I_f , Fig. 9 shows that an

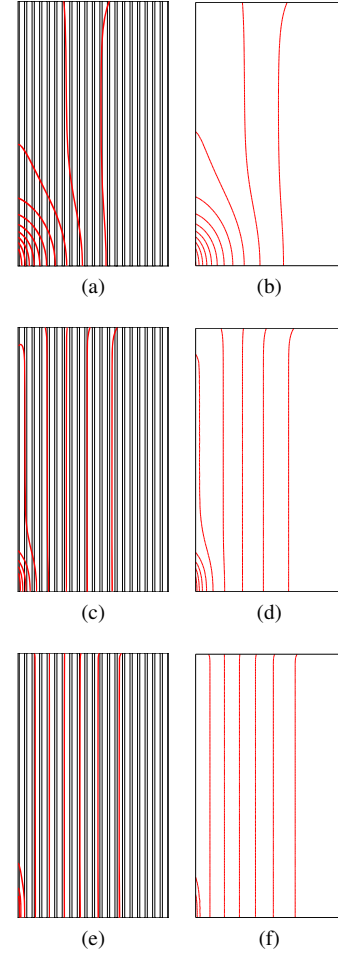


Fig. 5. Flux lines in the foil-winding domain at $t = T/8$ (maximum voltage): (a) 200 Hz reference (b) 200 Hz homogenized (c) 2 kHz reference (d) 2 kHz homogenized (e) 20 kHz reference (f) 20 kHz homogenized.

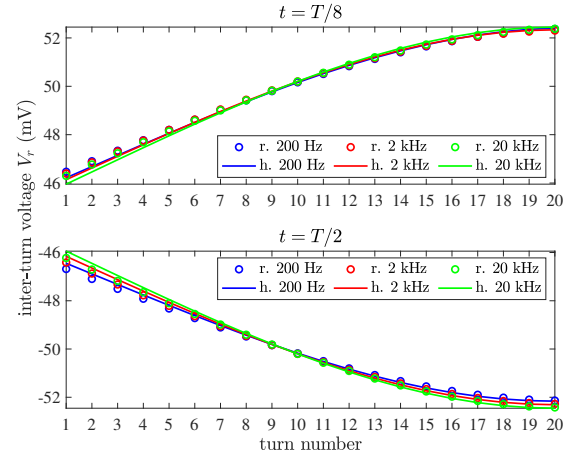


Fig. 6. Inter-turn voltage at $t = T/8$ and $t = T/2$ across the turns of the foil winding.

excellent correspondence is maintained even at 20 kHz. This behavior is explained by the inductive behavior of the device as shown in Fig 5.

Fig. 10 shows how the Joule losses vary with time. An excellent agreement is obtained at 200 Hz with an L2-error

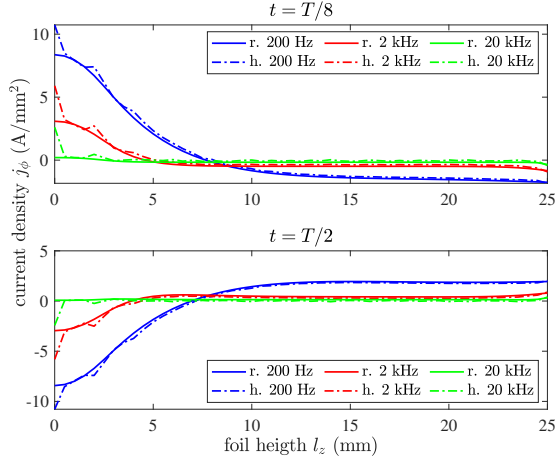


Fig. 7. Current density along half-height of the first turn ($1/20$) at $t = T/8$ and $t = T/2$.

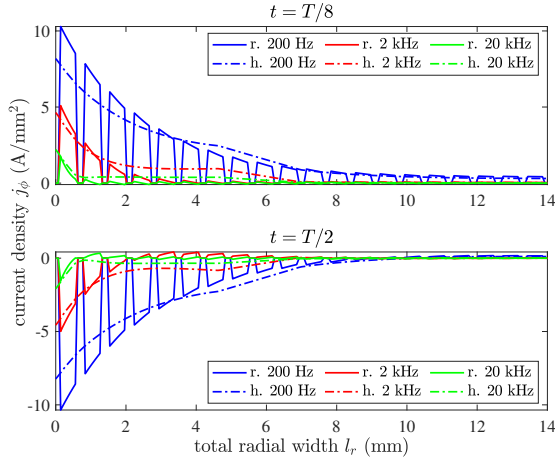


Fig. 8. Current density along the total radial width l_r at $t = T/8$ and $t = T/2$ for $z = 0$.

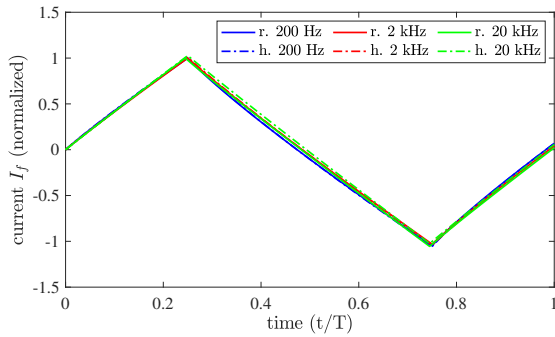


Fig. 9. Current I_f vs normalized time (one period). Values normalized with respect to the maximum reference values: 10.4 A, 1.2 A, 0.13 A for 200 Hz, 2 kHz and 20 kHz, respectively.

ϵ , over the complete period, of 2.2%. Similar results are obtained for 2 kHz, but ϵ increases to 5.3%. The Joule losses are considerably worsened at 20 kHz with ϵ reaching a value of 29.4%; linked to the overestimated terminal resistance from $\zeta = 0.75$ on. The error ϵ is measured with the L2-norm of the difference between the reference p_r and the homogenized p_h

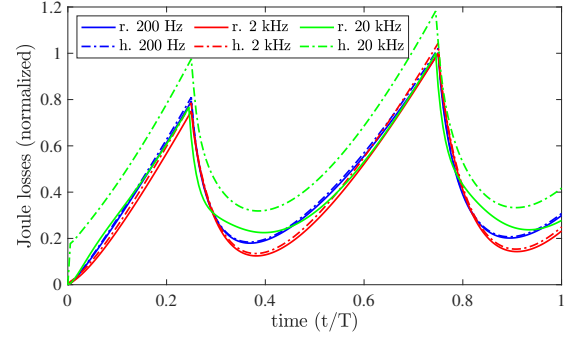


Fig. 10. Joule losses vs normalized time (one period). Values normalized with respect to the maximum reference values: 1.41 W, 103 mW, 5.31 mW for 200 Hz, 2 kHz and 20 kHz, respectively.

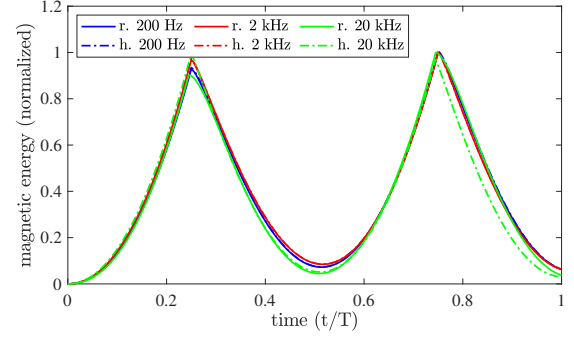


Fig. 11. Magnetic energy vs normalized time (one period). Values normalized with respect to the maximum reference values: 7.5 mJ, 9.4 μ J, 75.3 pJ for 200 Hz, 2 kHz and 20 kHz, respectively.

losses in a period i.e.

$$\epsilon = \frac{\|p_r - p_h\|_2}{\|p_r\|_2}. \quad (17)$$

The magnetic energy as a function of time is presented in Fig. 11. An excellent accuracy is obtained for the 200 Hz and 2 kHz cases. At 20 kHz, the homogenization follows the reference except for the last quarter of period where the homogenized curve falls below it.

In the preceding analysis, instantaneous comparisons are made at $t = T/8$ and $t = T/2$ corresponding to peak positive and negative values of the applied voltage V , yet similar results are obtained for the remaining instants. In general, the proposed time-domain extension confirms the excellent accuracy of the homogenized model at low frequencies already presented for the frequency domain in [10], [11]. At higher frequencies, the precision gets highly reduced caused by the inability of the model to correctly represent the Joule losses. The air-gap effect does not affect the accuracy of the homogenized model at low frequencies, however its fringing flux is a source of disturbances that worsens the behavior at high frequencies, specially for the Joule losses.

To establish the influence of the homogenized mesh in the precision of the results, we compare in Table I the L2-error ϵ (calculated for the Joule losses), the corresponding computational time $t_{\Delta t}$ and the speed-up factor sp for N_u varying from 1 to 3 at all frequencies. A mesh with $N_u = 1$ results in inaccurate results even at 200 Hz. For $N_u = 2$, as

TABLE I
PERFORMANCE OF THE HOMOGENIZED MODEL

f	N_u	ϵ (%)	$t_{\Delta t}$ (ms)	sp
200 Hz	1	7.5	10	538.9
	2	2.2	31	173.8
	3	1.3	70	77
2 kHz	1	27.1	10	538.9
	2	4.7	31	173.8
	3	2.1	70	77
20 kHz	1	183.9	22	245
	2	29.4	70	77
	3	5.7	221	24.4

discussed before, an excellent accuracy is obtained at 200 Hz and decreases as the frequency increases. Refining the mesh to $N_u = 3$ results in excellent accuracy for 2 kHz, but an error of 5.7% is still found at 20 kHz. Evidently, as N_u increases, $t_{\Delta t}$ increases as well; however, same times are obtained for 200 Hz and 2 kHz.

V. CONCLUSIONS

A method has been proposed for the time-domain homogenization of foil windings. It allows to solve the eddy-current problem in a 2-D axisymmetric FE model with excellent accuracy and reasonable computational cost at low frequencies. At higher frequencies, the method becomes imprecise due to its inability to correctly represent the Joule losses in the foil-winding region. Further work is required to improve the high-frequency eddy-current effects in the model. The fringing flux does not affect the accuracy of the model at low frequencies, but it worsens the results at high frequencies. Below f_{max} , a refinement of the mesh may improve the accuracy of the results at the expense of a higher computational time. This method can be straightforwardly applied to 3-D FE models to account for different device shapes.

REFERENCES

- [1] P. L. Dowell, "Effects of eddy currents in transformer windings," *Proc. IEE*, vol. 113, no. 8, pp. 1387-1394, 1966.
- [2] J. A. Ferreira, "Electromagnetic modelling of power electronic converters," *Springer Science & Business Media*, 1989.
- [3] R. P. Wojda and M. K. Kazimierczuk, "Magnetic Field Distribution and Analytical Optimization of Foil Windings Conducting Sinusoidal Current," *IEEE Magnetics Letters*, vol. 4, 2013.
- [4] G. Diaz and E. Mombello, "Semianalytic Integral Method for Fast Solution of Current Distribution in Foil Winding Transformers," *IEEE Trans. Magn.*, vol. 51, no. 9, pp. 1-9, 2015.
- [5] F. Robert, P. Mathys, B. Velaerts and J-P. Schauwers, "Two-dimensional analysis of the edge effect field and losses in high-frequency transformer foils," *IEEE Trans. Magn.*, vol. 41, no. 8, pp. 2377-2383, Aug. 2005.
- [6] I. Kovačević-Badstübner, R. Burkart, C. Dittli, J. W. Kolar and A. Musing, "A fast method for the calculation of foil winding losses," *2015 17th European Conference on Power Electronics and Applications (EPE'15 ECCE-Europe)*, Geneva, 2015, pp. 1-10.
- [7] C. R. Sullivan, "Computationally efficient winding loss calculation with multiple windings, arbitrary waveforms, and two-dimensional or three-dimensional field geometry," *IEEE Trans. Power Electron.*, vol. 16, no. 1, pp. 142-150, Jan. 2001.
- [8] D. Leuenberger and J. Biela, "Semi-numerical method for loss-calculation in foil-windings exposed to an air-gap field," *2014 International Power Electronics Conference (IPEC-Hiroshima 2014 - ECCE ASIA)*, Hiroshima, 2014, pp. 868-875.
- [9] M. T. Villen, J. Letosa, A. Nogues and I. Murillo, "Procedure to Accelerate Calculations of Additional Losses in Transformer Foil Windings," *Electric Power Systems Research*, vol. 95, pp. 85-89, 2013.

- [10] H. De Gerssem and K. Hameyer, "A Finite Element Model for Foil Winding Simulation," *IEEE Trans. Magn.*, vol. 37, pp. 3427-3432, Sept. 2001.
- [11] P. Dular and C. Geuzaine, "Spatially Dependent Global Quantities Associated With 2-D and 3-D Magnetic Vector Potential Formulations for Foil Winding Modeling," *IEEE Trans. Magn.*, vol. 38, no. 2, pp. 633-636, March 2002.
- [12] K. H. Nasser, and D. M. Divan, "Optimal air-gap design in high-frequency foil windings," *IEEE Trans. Power Electron.*, Vol. 13, no. 5, pp. 942-949, 1998.
- [13] R. Jez, "Influence of the Distributed Air Gap on the Parameters of an Industrial Inductor," *IEEE Trans. Magn.*, vol. 53, no. 11, pp. 1-5, Nov. 2017.
- [14] C. A. Valdivieso, *et al.*, "Time-Domain Homogenization of Foil Windings in 2-D Magnetodynamic Finite-Element Models," *2019 2nd International Conference on the Computation of Electromagnetic Fields (COMPUMAG)*, Paris, France, 2019.
- [15] P. Lombard and G. Meunier, "A general purpose method for electric and magnetic combined problems for 2D, axisymmetric and transient systems," *IEEE Trans. Magn.*, vol. 29, no. 2, pp. 1737-1740, March 1993.
- [16] *Altair FluxTM*. (2019.1), Altair Engineering. Accessed: Jan. 20, 2020. [Online]. Available: <https://www.altair.com/flux/>
- [17] C. A. Balanis, *Advanced Engineering Electromagnetics*. Hoboken, New Jersey: John Wiley & Sons, Inc., 2012, p. 18-21.
- [18] G. Meunier, *The finite element method for electromagnetic modeling*. Hoboken, New Jersey: John Wiley & Sons, Inc., 2010, p. 510-541.